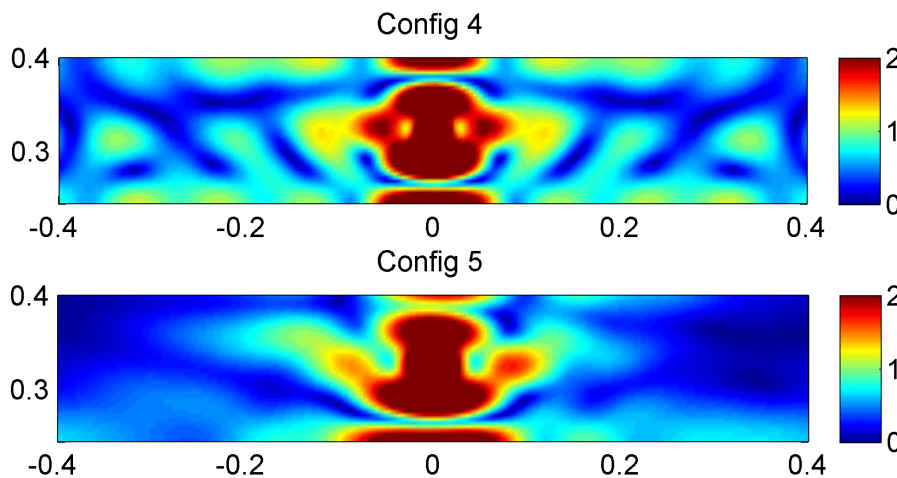




## Executive summary

# Green's functions for in-duct beamforming applications

AIAA Paper 2012-2248

**Report no.**

NLR-TP-2012-248

**Author(s)**

P. Sijtsma

**Report classification**

UNCLASSIFIED

**Date**

July 2012

**Knowledge area(s)**

Aëro-akoestisch en experimenteel  
aërodynamisch onderzoek

**Descriptor(s)**

Engine Noise  
Microphone Arrays

**Problem area**

This paper considers Green's functions of the acoustic differential equation in axisymmetric parallel shear flows. Green's functions are solutions of linear differential equations with a Dirac-delta function in the right hand side. In acoustics, they can be considered as expressions for the field generated by monopole sources.

**Description of work**

The Green's functions are evaluated in the frequency-domain, and expressed in azimuthal modes. For each mode the governing equation is Fourier-transformed to the axial wave number domain, and the remaining ordinary differential equation in the radial coordinate is

solved. Then, the inverse Fourier transform to the physical axial coordinate is applied to obtain the final solution. Instead of applying the Residue Theorem to get a solution in terms of duct modes, the Fourier integral is evaluated numerically. Emphasis is put on the practical aspects of calculating the Green's function. The key assumption made here is that the flow properties are stepwise constant in radial direction. In other words, the shear flow is represented by a set of cylindrical vortex sheets. Thus, issues with continuum modes are circumvented.

**Results and conclusions**

The Green's functions can be calculated in a straightforward way.

**Applicability**

This paper is motivated by in-duct applications, but the method described here can also be applied to sources in unducted sheared flows, e.g., to model sound refraction by the shear layer of a

circular open jet or, or to model diffraction and refraction of sound in the presence of a cylindrical fuselage.



NLR-TP-2012-248

## Green's functions for in-duct beamforming applications

AIAA Paper 2012-2248




P. Sijtsma

This report is based on a presentation held at the 18th AIAA/CEAS Aeroacoustics Conference, Colorado Springs, CO, USA, 4-6 June 2012.

The contents of this report may be cited on condition that full credit is given to NLR and the authors.  
This publication has been refereed by the Advisory Committee AEROSPACE VEHICLES.

Customer	National Aerospace Laboratory NLR
Contract number	GA 213411
Owner	National Aerospace Laboratory NLR
Division NLR	Aerospace Vehicles
Distribution	Unlimited
Classification of title	Unclassified
	July 2012

Approved by:

Author P. Sijtsma 	Reviewer M. Tuinstra 	Managing department J. Hakkaart 
Date: 6-8-2012	Date: 7-8-2012	Date: 9-8-'12

## Contents

<b>Nomenclature</b>	<b>3</b>
<b>I. Introduction</b>	<b>4</b>
<b>II. Theory</b>	<b>5</b>
A. Governing equations	5
B. Solution procedure	6
C. Inverse Fourier transform	6
<b>III. Conditions at inner and outer radius</b>	<b>7</b>
A. Wall condition at outer radius	7
B. Free-field condition at outer radius	7
C. Wall condition at inner radius	7
D. No-hub condition at inner radius	7
E. Non-locally reacting liners	8
<b>IV. Stepwise uniform flow</b>	<b>8</b>
A. Governing equations	8
B. Interface conditions	9
C. Shooting procedure	9
D. Properties of wave number solution	9
<b>V. Numerical Examples</b>	<b>10</b>
<b>VI. Conclusion</b>	<b>14</b>
<b>Appendix: Source on the axis</b>	<b>14</b>
<b>Acknowledgments</b>	<b>14</b>
<b>References</b>	<b>15</b>

# Green's Functions for In-Duct Beamforming Applications

Pieter Sijtsma \*

*National Aerospace Laboratory NLR, 8300 AD Emmeloord, The Netherlands*

This paper considers the calculation of Green's functions in a ducted parallel shear flow, in which both the flow speed and the temperature vary in radial direction. The duct can be hollow or annular. Wall lining can be locally or non-locally reacting. For annular ducts, the hub may be lined as well. The Green's function is evaluated in the frequency-domain, and expressed in azimuthal modes. For each mode the governing equation is Fourier-transformed to the axial wave number domain, and the remaining ordinary differential equation in the radial coordinate is solved. Then, the inverse Fourier transform to the physical axial coordinate is applied to obtain the final solution. Instead of applying the Residue Theorem to get a solution in terms of duct modes, the Fourier integral is evaluated numerically. Emphasis is put on the practical aspects of calculating the Green's function. The key assumption made here is that the flow properties are stepwise constant in radial direction. In other words, the shear flow is represented by a set of cylindrical vortex sheets. Thus, issues with continuum modes are circumvented, and the Green's function can be calculated in a straightforward way.

## Nomenclature

$A$	= constant for Bessel function
$B$	= constant for Hankel function
$c_0$	= ambient sound speed
$d$	= liner thickness
$F$	= axial Fourier transform of $G$
$F_m$	= axial Fourier transform of $G_m$
$f$	= frequency
$\vec{f}$	= force field
$G$	= Green's function
$G_m$	= azimuthal mode of $G$
$H_m^{(2)}$	= $m$ -th order Hankel function of the second kind
$i$	= imaginary unit
$J$	= number of flow intervals
$J_m$	= $m$ -th order Bessel function of the first kind
$j$	= flow interval number
$N$	= number of eigenvalues on the real axis
$m$	= azimuthal mode number
$p$	= acoustic pressure
$Q_j$	= see Eq. (38)
$R$	= gas constant
$R_{\text{inner}}$	= inner radius
$R_{\text{outer}}$	= outer radius
$r$	= radial coordinate
$r_j$	= radial position of vortex sheet
$T_0$	= ambient temperature
$t$	= time
$U$	= parallel main flow velocity

\* Senior Scientist, Department of Helicopters & Aeroacoustics, P.O. Box 153, Member AIAA.

$u$	= inner solution
$v$	= outer solution
$X_a, X_b$	= auxiliary functions, see Eq. (42)
$x$	= axial coordinate
$Z_c$	= characteristic impedance of porous material
$Z_{fs}$	= facing sheet impedance
$Z_{inner}$	= impedance at inner wall
$Z_{outer}$	= impedance at outer wall
$\alpha$	= axial wave number
$\alpha_{m\mu}$	= axial eigenvalue
$\delta$	= Dirac-delta function
$\varepsilon$	= radial wave number
$\phi$	= azimuthal coordinate of source
$\gamma$	= ratio of specific heats
$\mu_p$	= propagation constant of porous material
$\Theta_{inner}$	= right hand side of Eq. (20) or Eq. (22)
$\Theta_{outer}$	= right hand side of Eq. (15) or Eq. (19)
$\theta$	= azimuthal coordinate
$\rho$	= radial coordinate of source
$\rho_0$	= air density
$\sigma$	= volume source strength
$\tau$	= source emission time
$\omega$	= angular frequency
$\xi$	= axial coordinate of source

## I. Introduction

THIS paper discusses Green's functions of the acoustic differential equation in axisymmetric parallel shear flows. Green's functions are solutions of linear differential equations with a Dirac-delta function in the right hand side. In acoustics, they can be considered as expressions for the field generated by monopole sources. This paper is motivated by in-duct applications<sup>1</sup>, but the method described here can also be applied to sources in unducted sheared flows, e.g., to model sound refraction by the shear layer of a circular open jet of, or to model diffraction and refraction of sound in the presence of a cylindrical fuselage.

Green's functions can be useful for several in-duct applications:

- calculation of the total acoustic field when volume sources and/or dipole sources on a surface are given, e.g., in lifting surface theory<sup>2,3</sup> or in the Ffowcs Williams-Hawkings method<sup>4,5</sup>,
- testing CAA codes<sup>6</sup>,
- constructing steering vectors for in-duct beamforming<sup>7,8</sup>.

Moreover, if wall lining is included, Green's functions can be used to optimize liners.

An analytic expression, in terms of duct modes, for the Green's function in an annular duct with uniform flow and hard walls, is already known for a few decades<sup>3</sup>. More recently, analytic expressions were developed for uniform flow and locally-reacting liners<sup>9</sup>. This paper considers the more general case of a ducted parallel shear flow, in which the flow speed and the temperature may vary in radial direction. The duct can be either hollow or annular. Wall lining can be locally or non-locally reacting. In annular ducts, the hub may be lined as well.

Just like the existing expressions referenced above, the Green's function is evaluated in the frequency-domain, and expressed in azimuthal modes. For each mode the governing equation is Fourier-transformed to the axial wave number domain, and the remaining ordinary differential equation in the radial coordinate is solved. Then, the inverse Fourier transform to the physical axial coordinate is applied to obtain the final solution. Instead of applying the Residue Theorem to get a solution in terms of duct modes<sup>9</sup>, the Fourier integral is evaluated numerically. The frequency-domain approach ignores issues associated with unstable acoustic modes<sup>10-12</sup>.

Emphasis is put on the practical aspects of calculating the Green's function. The key assumption made here is that the flow properties are stepwise constant in radial direction. In other words, the shear flow is represented by a set of cylindrical vortex sheets. This offers a number of benefits:

- The solution in the frequency-wave number domain can be expressed in terms of Bessel functions. Well-known asymptotic expansions can be used for large arguments.
- For a ducted flow, the frequency-wave number solution is meromorphic. There are no “branch cuts”.
- Its poles are related to acoustic modes. There are neither continuum modes nor convection modes.

A more in-depth study on the effects of flow gradients was recently performed by Brambley, Darau, and Rienstra<sup>13</sup>.

The organization of this paper is as follows. Chapter II provides a general overview of the problem and the solution procedure. Chapter III gives an overview of the boundary conditions. Chapter IV discusses the implications of a stepwise uniform flow. Chapter V shows a number of typical examples.

## II. Theory

In the theory that follows, all physical quantities are in full dimensions. To avoid confusion, they were not made dimensionless, as the sound speed and the air density do not need to be uniform. Cylindrical coordinates  $(x, r, \theta)$  will be used.

### A. Governing equations

The following linearized expression can be derived<sup>14</sup> for the acoustic pressure  $p$  in a parallel shear flow:

$$\frac{D}{Dt} \left( \nabla \cdot (T_0 \nabla p) - \frac{1}{\gamma R} \frac{D^2 p}{Dt^2} \right) - 2T_0 \frac{dU}{dr} \frac{\partial^2 p}{\partial r \partial x} = \frac{D}{Dt} \left( \nabla \cdot (T_0 \vec{f}) - \rho_0 T_0 \frac{D\sigma}{Dt} \right) - 2T_0 \frac{dU}{dr} \frac{\partial f_r}{\partial x}. \quad (1)$$

Herein, we have:

- $\rho_0$  : the air density,
- $T_0$  : the static temperature,
- $\gamma$  : the ratio between specific heats (in air: 1.4),
- $R$  : the gas constant (in air:  $287 \text{ m}^2 \text{ s}^{-2} \text{ K}^{-1}$ ),
- $U$  : the axial velocity,
- $\vec{f}$  : an external fluctuating force field acting on the fluid,
- $\sigma$  : external fluctuating volume sources.

The static temperature  $T_0$  and the axial velocity  $U$  can be dependent on the radial coordinate  $r$ , having any subsonic profile. The sound speed  $c_0$  follows from

$$c_0^2 = \gamma R T_0. \quad (2)$$

The convective derivative is

$$\frac{D}{Dt} = \frac{\partial}{\partial t} + U \frac{\partial}{\partial x}. \quad (3)$$

We consider the following differential equation for the Green's function  $G$ :

$$\frac{D}{Dt} \left( \nabla \cdot (T_0 \nabla G) - \frac{1}{\gamma R} \frac{D^2 G}{Dt^2} \right) - 2T_0 \frac{dU}{dr} \frac{\partial^2 G}{\partial r \partial x} = T_0 \frac{D}{Dt} \delta(t - \tau) \delta(x - \xi) \delta(y - \eta) \delta(z - \zeta). \quad (4)$$

This is the equivalent of the Green's function in uniform flow<sup>2,9</sup>. Solutions of Eq. (4) can be used to construct solutions of Eq. (1), under the condition that the second term in the right hand side is zero:

$$\frac{dU}{dr} \frac{\partial f_r}{\partial x} = 0. \quad (5)$$

Hence, forces with a radial component, acting on a shear flow, are excluded by this description. In Chapter IV, we will consider flows with piecewise constant velocity. Then, condition (5) is valid when the force is not acting on a vortex sheet.

After performing the Fourier transforms  $t \rightarrow \omega$  and  $x \rightarrow \alpha$  we find for (4)

$$T_0 \left( \frac{1}{r} \frac{\partial}{\partial r} r \frac{\partial}{\partial r} + \frac{1}{r^2} \frac{\partial^2}{\partial \theta^2} \right) F - \left( \frac{2\alpha T_0}{\omega + U\alpha} \frac{dU}{dr} - \frac{dT_0}{dr} \right) \frac{\partial F}{\partial r} + \left( \frac{1}{\gamma R} (\omega + U\alpha)^2 - T_0 \alpha^2 \right) F = T_0 \delta(y - \eta) \delta(z - \zeta). \quad (6)$$

Herein, the axial Fourier transform is defined by

$$F(\alpha) = \int_{-\infty}^{\infty} \exp[-i\alpha(x - \xi)] G(x) dx. \quad (7)$$

Substituting

$$F(\alpha, r, \theta, \rho, \phi) = \sum_{m=-\infty}^{\infty} \exp[-im(\theta - \phi)] F_m(\alpha, r, \rho), \quad (8)$$

and writing the source position in cylinder coordinates  $(\xi, \rho, \phi)$ , we obtain

$$\frac{T_0}{r} \frac{d}{dr} r \frac{dF_m}{dr} - \left( \frac{2\alpha T_0}{\omega + U\alpha} \frac{dU}{dr} - \frac{dT_0}{dr} \right) \frac{dF_m}{dr} + \left( \frac{1}{\gamma R} (\omega + U\alpha)^2 - T_0 \left( \alpha^2 + \frac{m^2}{r^2} \right) \right) F_m = \frac{T_0}{2\pi\rho} \delta(r - \rho). \quad (9)$$

In the left hand side of Eq. (9) we recognize the Pridmore-Brown wave operator<sup>15</sup>. We can rewrite Eq. (9) in a self-adjoint form:

$$\frac{1}{r} (\omega + U\alpha)^2 \frac{d}{dr} \left( \frac{r \frac{dF_m}{dr} T_0}{(\omega + U\alpha)^2} \right) + \left( \frac{1}{\gamma R} (\omega + U\alpha)^2 - T_0 \left( \alpha^2 + \frac{m^2}{r^2} \right) \right) F_m = \frac{T_0}{2\pi\rho} \delta(r - \rho). \quad (10)$$

## B. Solution procedure

It is assumed that an inner radius  $R_{\text{inner}}$  and an outer radius  $R_{\text{outer}}$  exist, such that

$$0 < R_{\text{inner}} \leq \rho \leq R_{\text{outer}}. \quad (11)$$

Obviously, this excludes sources on the axis, i.e., when  $\rho = 0$ . This special case is treated in the appendix.

Suppose that the ratio between  $F_m$  and  $dF_m/dr$  is known at  $r = R_{\text{inner}}$  and  $r = R_{\text{outer}}$ . Then Eq. (10) can be solved by a “shooting” method: First, an “inner solution”  $u(r)$  for  $R_{\text{inner}} \leq r \leq \rho$  and an “outer solution”  $v(r)$  for  $\rho \leq r \leq R_{\text{outer}}$  are constructed, which satisfy the homogeneous equation and the boundary conditions at  $r = R_{\text{inner}}$  and  $r = R_{\text{outer}}$ , respectively. By applying the appropriate relations between inner and outer solution at  $r = \rho$ , i.e., continuity and a prescribed jump in the derivative, the full solution of Eq. (10) is found to be

$$F_m(\alpha, r, \rho) = \frac{1}{2\pi\rho(u(\rho)v'(\rho) - u'(\rho)v(\rho))} \times \begin{cases} v(\rho)u(r), & r < \rho, \\ u(\rho)v(r), & r > \rho. \end{cases} \quad (12)$$

Then  $G_m$  is obtained by performing the inverse Fourier transform:

$$G_m(x, r, \xi, \rho) = \frac{1}{2\pi} \int_{-\infty}^{\infty} \exp[i\alpha(x - \xi)] F_m(\alpha, r, \rho) d\alpha, \quad (13)$$

and the full solution is given by

$$G(x, r, \theta, \xi, \rho, \phi) = \sum_{m=-\infty}^{\infty} \exp[-im(\theta - \phi)] G_m(x, r, \xi, \rho). \quad (14)$$

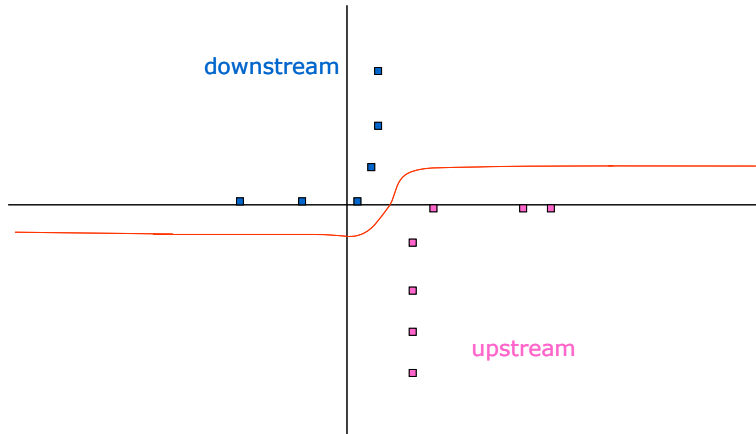


Figure 1. Possible locations of singularities of  $F_m$  in the complex  $\alpha$ -plane, and integration contour.

## C. Inverse Fourier transform

In order to obtain the final solution, we need to (numerically) evaluate the Fourier integrals, Eq. (13). However, there are  $\alpha$ -values for which the denominator in Eq. (12) is zero. These are the so-called eigenvalues  $\alpha_{m\mu}$ , which



can be shown to be independent of  $\rho$ . Around isolated eigenvalues,  $F_m$  behaves like  $1/(\alpha - \alpha_{m\mu})$ . A sketch of possible eigenvalues is made in Figure 1, where it is assumed that  $U \geq 0$ . Generally, the eigenvalues are complex-valued, but a number of them may be located on the real axis (i.e., in the case of hard-wall boundary conditions; see next chapter). In a strict sense, this would make the Fourier integrals, Eq. (13), nonexistent. Nevertheless, we can evaluate them by moving the integration contour into the complex plane, as sketched in Figure 1.

### III. Conditions at inner and outer radius

#### A. Wall condition at outer radius

If the outer radius  $R_{\text{outer}}$  of the previous chapter is the radius of a flow duct, then Myers' boundary condition<sup>16</sup> can be imposed:

$$\frac{dF_m}{dr} = \frac{\rho_0 (\omega + U\alpha)^2}{i\omega Z_{\text{outer}} F_m}. \quad (15)$$

Herein  $Z_{\text{outer}}$  is the wall impedance. In the case of a hard wall, we have  $Z_{\text{outer}} = \infty$ .

#### B. Free-field condition at outer radius

A free-field condition can be derived by assuming that the flow properties are uniform for  $r \geq R_{\text{outer}}$ . Then Eq. (10) simplifies into

$$\frac{1}{r} \frac{d}{dr} \left( r \frac{dF_m}{dr} \right) + (\varepsilon^2 - m^2/r^2) F_m = 0, \quad (16)$$

with

$$\varepsilon = -i \left( \alpha^2 - (\omega + U\alpha)^2 / c_0^2 \right)^{1/2}. \quad (17)$$

Equation (16) is Bessel's equation<sup>17</sup>. The solution that vanishes for  $r \rightarrow \infty$  is

$$F_m = H_m^{(2)}(\varepsilon r), \quad (18)$$

where  $H_m^{(2)}$  is the  $m$ -th order Hankel function of the second kind. Consequently, at  $r = R_{\text{outer}}$  we have

$$\frac{dF_m}{dr} = \frac{\varepsilon H_m^{(2)'}(\varepsilon R_{\text{outer}})}{H_m^{(2)}(\varepsilon R_{\text{outer}})} F_m. \quad (19)$$

#### C. Wall condition at inner radius

If the inner radius  $R_{\text{inner}}$  is the radius of a center body (hub), then again Myers' boundary condition can be imposed:

$$\frac{dF_m}{dr} = -\frac{\rho_0 (\omega + U\alpha)^2}{i\omega Z_{\text{inner}} F_m}, \quad (20)$$

with  $Z_{\text{inner}}$  the wall impedance. Note the sign change with respect to Eq. (15).

#### D. No-hub condition at inner radius

If there is no hub, we assume uniform flow conditions for  $r \leq R_{\text{inner}}$ . Then again Eq. (16) holds. The solution that is bounded for  $r \rightarrow 0$  is

$$F_m = J_m(\varepsilon r), \quad (21)$$

where  $J_m$  is the  $m$ -th order Bessel function. Consequently, at  $r = R_{\text{inner}}$  we have

$$\frac{dF_m}{dr} = \frac{\varepsilon J_m'(\varepsilon R_{\text{inner}})}{J_m(\varepsilon R_{\text{inner}})} F_m. \quad (22)$$

### E. Non-locally reacting liners

For locally-reacting liners, the wall impedances  $Z_{\text{outer}}$  and  $Z_{\text{inner}}$  are independent of the axial wave number  $\alpha$ . However, in the approach described above, there is no need for that restriction. In other words, we may use  $\alpha$ -dependent expressions for the wall impedance. Herewith, several types of non-locally reacting liners (“bulk-absorbers”) can be considered.

For a certain class of bulk-absorbers, the wall impedance can be written as<sup>18,19</sup>

$$Z_{\text{outer}} = Z_{\text{fs}} - i\mu_p Z_c \frac{J_m(\varepsilon R_{\text{outer}}) H_m^{(2)'}(\varepsilon(R_{\text{outer}} + d)) - H_m^{(2)}(\varepsilon R_{\text{outer}}) J_m'(\varepsilon(R_{\text{outer}} + d))}{\varepsilon \left\{ J_m'(\varepsilon R_{\text{outer}}) H_m^{(2)'}(\varepsilon(R_{\text{outer}} + d)) - H_m^{(2)'}(\varepsilon R_{\text{outer}}) J_m'(\varepsilon(R_{\text{outer}} + d)) \right\}}, \quad (23)$$

$$Z_{\text{inner}} = Z_{\text{fs}} + i\mu_p Z_c \frac{J_m(\varepsilon R_{\text{inner}}) H_m^{(2)'}(\varepsilon(R_{\text{inner}} - d)) - H_m^{(2)}(\varepsilon R_{\text{inner}}) J_m'(\varepsilon(R_{\text{inner}} - d))}{\varepsilon \left\{ J_m'(\varepsilon R_{\text{inner}}) H_m^{(2)'}(\varepsilon(R_{\text{inner}} - d)) - H_m^{(2)'}(\varepsilon R_{\text{inner}}) J_m'(\varepsilon(R_{\text{inner}} - d)) \right\}}. \quad (24)$$

Herein, we have:

- $Z_{\text{fs}}$  : facing sheet impedance,
- $d$  : liner thickness ,
- $\mu_p$  : propagation constant of porous material,
- $Z_c$  : characteristic impedance of porous material.

Obviously, the properties of the inner and the outer liner may be different. The radial wave number in porous material is given by

$$\varepsilon^2 = \mu_p^2 - \alpha^2. \quad (25)$$

## IV. Stepwise uniform flow

### A. Governing equations

Instead of smoothly varying shear flow properties  $U(r)$ ,  $T_0(r)$ , and  $c_0(r)$ , we now consider a flow which is stepwise uniform. That is, we subdivide the duct in radial direction into  $J$  intervals:

$$r_{j-1} \leq r < r_j, j = 0, \dots, J, \quad (26)$$

with

$$\begin{cases} r_0 = R_{\text{inner}}, \\ r_J = R_{\text{outer}}. \end{cases} \quad (27)$$

In each interval  $r_{j-1} \leq r < r_j$  constant flow properties  $U_j$ ,  $T_{0,j}$ , and  $c_{0,j}$  are assumed. The source is supposed to be located in one of the intervals. Its position may be exactly on a shear layer ( $\rho = r_j$ ), but then one of the corresponding intervals needs to be allocated for containing the source.

Instead of Eq.(10), we now need to solve

$$\frac{1}{r} \frac{d}{dr} r \frac{dF_{m,j}}{dr} + \left( \varepsilon_j^2 - \frac{m^2}{r^2} \right) F_{m,j} = \frac{1}{2\pi\rho} \delta(r - \rho) \quad (28)$$

in the interval that contains the source, and

$$\frac{1}{r} \frac{d}{dr} r \frac{dF_{m,j}}{dr} + \left( \varepsilon_j^2 - \frac{m^2}{r^2} \right) F_{m,j} = 0 \quad (29)$$

elsewhere. In Eqs. (28) and (29) we have introduced

$$\varepsilon_j = -i \left( \alpha^2 - (\omega + U_j \alpha)^2 / c_{0,j}^2 \right)^{1/2}. \quad (30)$$

An advantage of this approach is that we can describe the solutions of Eq. (29) in terms of Bessel functions. Thus, numerical problems with Runge-Kutta solvers, which may occur at large values of  $\alpha$ , are avoided. Instead, asymptotic expression for Bessel functions can be used.

## B. Interface conditions

Across a vortex sheet at  $r = r_j$ , we prescribe continuity of pressure:

$$F_{m,j} = F_{m,j+1}. \quad (31)$$

The second interface condition can be derived easily from the self-adjoint form of the Pridmore-Brown operator, Eq. (10), yielding

$$\frac{\frac{dF_{m,j}}{dr} c_{0,j}^2}{(\omega + U_j \alpha)^2} = \frac{\frac{dF_{m,j+1}}{dr} c_{0,j+1}^2}{(\omega + U_{j+1} \alpha)^2}. \quad (32)$$

This is, in fact, the well-known “continuity of particle displacement” condition<sup>20,21</sup>.

## C. Shooting procedure

The “shooting” procedure mentioned in Section II.B is worked out as follows. First, an “inner solution”  $u(r)$  is constructed starting from the first interval  $r_0 \leq r \leq r_1$ . Here, the general solution can be written as

$$u_1(r) = AJ_m(\varepsilon_1 r) + BH_m^{(2)}(\varepsilon_1 r). \quad (33)$$

The constants  $A$  and  $B$  are fixed by setting

$$\begin{cases} u_1(r_0) = 1, \\ u_1'(r_0) = \Theta_{\text{inner}}, \end{cases} \quad (34)$$

where  $\Theta_{\text{inner}}$  is the right hand side of Eq. (20) or Eq. (22). Thus, we obtain

$$\begin{pmatrix} A \\ B \end{pmatrix} = \frac{\pi i r_0}{2} \begin{pmatrix} H_m^{(2)'}(\varepsilon_1 r_0) & -H_m^{(2)}(\varepsilon_1 r_0) \\ -J_m'(\varepsilon_1 r_0) & J_m(\varepsilon_1 r_0) \end{pmatrix} \begin{pmatrix} \varepsilon_1 \\ \Theta_{\text{inner}} \end{pmatrix}, \quad (35)$$

where use has been made of a Wronskian for Bessel functions<sup>17</sup>. If  $\rho \leq r_1$  we can evaluate by Eq. (33) the solution at the source location. Otherwise, we have to proceed to the next interval:  $r_{j-1} \leq r \leq r_j$ , with  $j = 2$ . As in Eq. (33) we write

$$u_j(r) = AJ_m(\varepsilon_j r) + BH_m^{(2)}(\varepsilon_j r). \quad (36)$$

At  $r = r_j$  we have the interface conditions Eqs. (31) and (32), which yield

$$\begin{cases} AJ_m(\varepsilon_j r_{j-1}) + BH_m^{(2)}(\varepsilon_j r_{j-1}) = u_{j-1}(r_{j-1}), \\ AJ_m'(\varepsilon_j r_{j-1}) + BH_m^{(2)'}(\varepsilon_j r_{j-1}) = Q_j u_{j-1}'(r_{j-1}) / \varepsilon_j, \end{cases} \quad (37)$$

with

$$Q_j = \frac{T_{0,j-1}(\omega + U_j \alpha)^2}{T_{0,j}(\omega + U_{j-1} \alpha)^2}. \quad (38)$$

Hence,

$$\begin{pmatrix} A \\ B \end{pmatrix} = \frac{\pi i r_{j-1}}{2} \begin{pmatrix} H_m^{(2)'}(\varepsilon_j r_{j-1}) & -H_m^{(2)}(\varepsilon_j r_{j-1}) \\ -J_m'(\varepsilon_j r_{j-1}) & J_m(\varepsilon_j r_{j-1}) \end{pmatrix} \begin{pmatrix} \varepsilon_j u_{j-1}(r_{j-1}) \\ Q_j u_{j-1}'(r_{j-1}) \end{pmatrix}. \quad (39)$$

We can repeat this until we arrive at the interval containing  $r = \rho$ .

The same procedure can be carried out for the “outer solution”  $v(r)$ . In that case we start with

$$\begin{cases} v_j(r_j) = 1, \\ v_j'(r_j) = \Theta_{\text{outer}}, \end{cases} \quad (40)$$

where  $\Theta_{\text{outer}}$  is the right hand side of Eq. (15) or Eq. (19). Thus, we obtain a total solution as in Eq. (12). The further evaluation is the same as outlined in Chapter II.

## D. Properties of wave number solution

The solution  $F_m(\alpha, r, \rho)$  is given by Eq. (12). The inverse Fourier transform, Eq. (13), needs to be applied in order to get the solution in physical coordinates. In this section some typical properties of  $F_m$  are discussed, when a ducted flow is considered (i.e., when condition (15) applies at  $r = R_{\text{outer}}$ ).

As mentioned in the previous section, the inner solution  $u(r)$  is constructed by shooting from  $r = r_0$  to  $r = \rho$ . Then, a number of radial intervals have to be passed through. Solutions per interval are given by insertion of Eq. (39) into Eq. (36), yielding

$$\begin{cases} u_j(r) = \frac{\pi i r_{j-1}}{2} (u_{j-1}(r_{j-1}) X_a(r) + Q_j u'_{j-1}(r_{j-1}) X_b(r)), \\ u'_j(r) = \frac{\pi i r_{j-1}}{2} (u_{j-1}(r_{j-1}) X'_a(r) + Q_j u'_{j-1}(r_{j-1}) X'_b(r)), \end{cases} \quad (41)$$

where

$$\begin{cases} X_a(r) = \varepsilon_j \left( H_m^{(2)'}(\varepsilon_j r_{j-1}) J_m(\varepsilon_j r) - J'_m(\varepsilon_j r_{j-1}) H_m^{(2)}(\varepsilon_j r) \right), \\ X_b(r) = -H_m^{(2)}(\varepsilon_j r_{j-1}) J_m(\varepsilon_j r) + J_m(\varepsilon_j r_{j-1}) H_m^{(2)}(\varepsilon_j r), \\ X'_a(r) = \varepsilon_j^2 \left( H_m^{(2)'}(\varepsilon_j r_{j-1}) J'_m(\varepsilon_j r) - J'_m(\varepsilon_j r_{j-1}) H_m^{(2)'}(\varepsilon_j r) \right), \\ X'_b(r) = \varepsilon_j \left( -H_m^{(2)}(\varepsilon_j r_{j-1}) J'_m(\varepsilon_j r) + J_m(\varepsilon_j r_{j-1}) H_m^{(2)'}(\varepsilon_j r) \right). \end{cases} \quad (42)$$

By inspection of the power series for Bessel functions<sup>17</sup>, it is seen that the functions defined in Eq. (42) are analytic in  $\varepsilon_j^2$ . Therefore, they are also analytic in  $\alpha$ . From Eq. (41) it follows that  $u_j(r)$  and  $u'_j(r)$  are meromorphic functions of  $\alpha$  if the same holds for  $u_{j-1}(r)$  and  $u'_{j-1}(r)$ . Iterating back to  $r = r_0$ , we can conclude that the inner solution  $u(r)$  is a meromorphic function of  $\alpha$  for any  $r$  between  $r_0$  and  $\rho$ , if the same is true for  $u_1(r_0)$  and  $u'_1(r_0)$ . From (34) it follows that this is indeed the case, since the right hand sides of Eqs. (20) and (22) are analytic expressions of  $\alpha$ .

Likewise, the outer solution  $v(r)$  is meromorphic, because this is also true for the right hand side of Eq. (15). It follows that  $F_m(\alpha, r, \rho)$ , Eq. (12), is a meromorphic function of  $\alpha$ . Thus, in principle, the integral in Eq. (13) can be evaluated by closing the contour in the upper or lower half plane (dependent on the sign of  $x - \xi$ ), and applying the Residue Theorem to the poles of  $F_m$ . For a uniform flow this has been evaluated by Rienstra and Tester<sup>8</sup>.

Note that this is not applicable to unducted flows, as the right hand side of Eq. (19) is not meromorphic. Then, branch cuts need to be defined<sup>13</sup>.

A further remark to be made is that the poles of  $F_m(\alpha)$  do not include convective modes. At first sight it looks as if (double) poles  $\alpha = -\omega/U_j$  are introduced in the inner and outer solution, through  $Q_j$  (see Eqs. (41) and (38)). These modes would form a discretized version of the “continuum modes”. However, poles like these in the numerator of the expression for  $F_m$ , Eq. (12), are completely counterbalanced by the same poles in the denominator.

## V. Numerical Examples

Green’s functions were calculated for 12 typical configurations. For all of them we had

- inner radius:  $R_{\text{inner}} = 0.244 \text{ m}$ ,
- outer radius:  $R_{\text{outer}} = 0.4 \text{ m}$ ,
- source position:  $\xi = 0 \text{ m}$ ,  $\rho = 0.32 \text{ m}$ ,  $\varphi = 2^\circ$ ,
- frequency:  $f = 4000 \text{ Hz}$ ,
- mean flow speed:  $U = 112 \text{ m/s}$ ,
- sound speed:  $c_0 = 340 \text{ m/s}$ .

In Table 1, an overview of the configurations is listed. An “open” casing or hub means that it is not present. For the “liner” configurations we used:

- outer impedance:  $Z_{\text{outer}}/\rho_0 c_0 = 1.5 - i$ ,
- inner impedance:  $Z_{\text{inner}}/\rho_0 c_0 = 2.5 - 2i$ .

For the “bulk” configurations we made use of Eqs. (23) and (24) for  $Z_{\text{outer}}$  and  $Z_{\text{inner}}$ , respectively, with:

- facing sheet impedance:  $Z_{\text{fs}}/\rho_0 c_0 = 0.5$ ,
- characteristic impedance:  $Z_c/\rho_0 c_0 = (1.5 + Y_{c_0}/i\omega)^{1/2}$ ,
- propagation constant:  $\mu_p = (1.5 + Y_{c_0}/i\omega)^{1/2} \omega/c_0$ .

The constant  $Y$  is the “resistivity” of the porous material, normalized by  $\rho_0 c_0$ , for which we used the value  $Y = 120 \text{ m}^{-1}$  (typical value for “Retimet”<sup>19</sup>). For the configuration with shear flow, the (piecewise uniform) flow profile is drawn in Figure 2. The temperature and, consequently, the sound speed were kept uniform.

**Table 1: Configurations for numerical examples**

	casing	hub	flow	intake SPL	exhaust SPL
Config 1	open	open	uniform	74.31	74.31
Config 2	open	hard	uniform	74.24	74.24
Config 3	hard	open	uniform	85.96	85.96
Config 4	hard	hard	uniform	85.68	85.68
Config 5	lined	hard	uniform	76.22	76.17
Config 6	hard	lined	uniform	82.38	82.71
Config 7	lined	lined	uniform	73.96	71.86
Config 8	lined	lined	shear	77.05	72.47
Config 9	bulk	hard	uniform	75.38	76.68
Config 10	hard	bulk	uniform	83.02	82.73
Config 11	bulk	bulk	uniform	73.08	71.94
Config 12	bulk	bulk	shear	77.67	72.70

The inverse Fourier transforms, Eq. (13), were calculated along contours

$$\alpha(s) = s_0 + s + \frac{is}{4} \exp \left\{ -\frac{1}{2} \left[ \left( \frac{c_0 s}{\omega} \right)^2 - 1 \right] \right\}, \quad -4 \frac{\omega}{c_0} \leq s \leq +4 \frac{\omega}{c_0}. \quad (43)$$

These contours cross the real axis in  $\alpha(0) = s_0$ . The  $s_0$ -values were obtained by searching hard-wall eigenvalues on the real axis. For each  $m$  this gives an even number (say  $N$ ) of eigenvalues. For a non-zero number of eigenvalues,  $s_0$  is chosen halfway eigenvalues  $N/2$  and  $N/2+1$ . If no eigenvalues are found, then an average value is chosen.

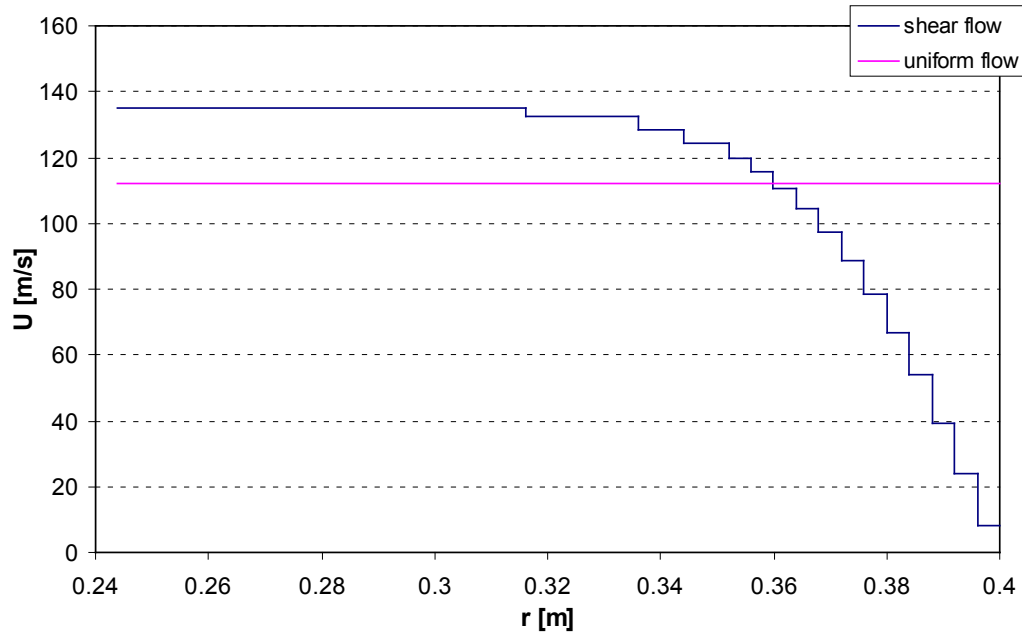


**Figure 2. Shear flow profile.**

For all configurations, the acoustic pressure amplitudes are plotted in the plane  $\theta = 0^\circ$ , which is very close to the source location. The results can be found in Figure 3 and Figure 4. The flow is from left to right. The mean SPL at the “intake” and “exhaust” positions  $x = -0.4$  and  $x = +0.4$ , respectively, are given in Table 1.

Clearly, shear flow, hub lining, and the liner type have a great impact. However, with a single frequency and a single source position, there is too little information to draw general conclusions. For a thorough study, a set of incoherent sources along a radial line would be required.

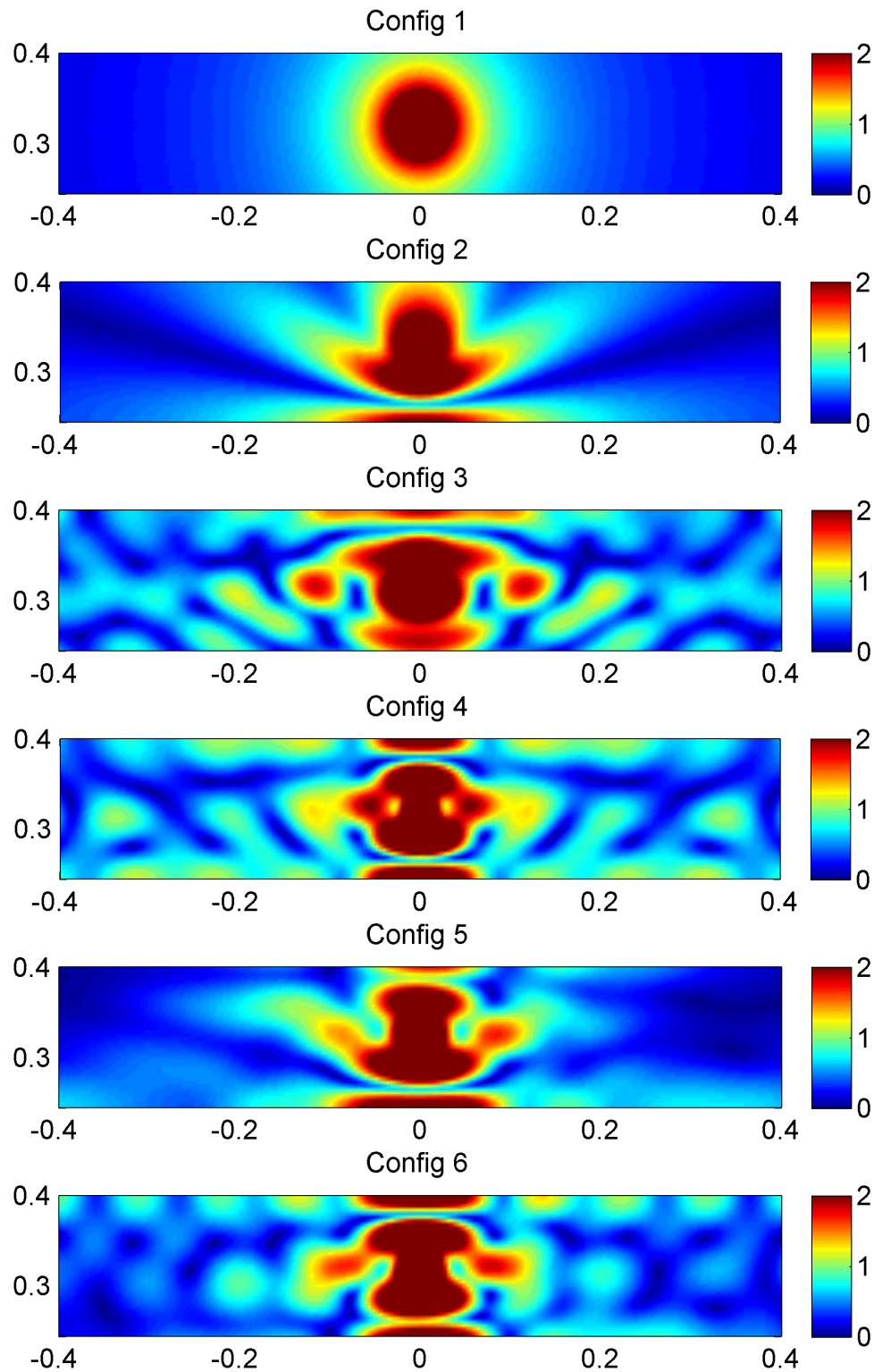


Figure 3. Acoustic pressure amplitude at  $\theta = 0^\circ$ , Configs 1-6.

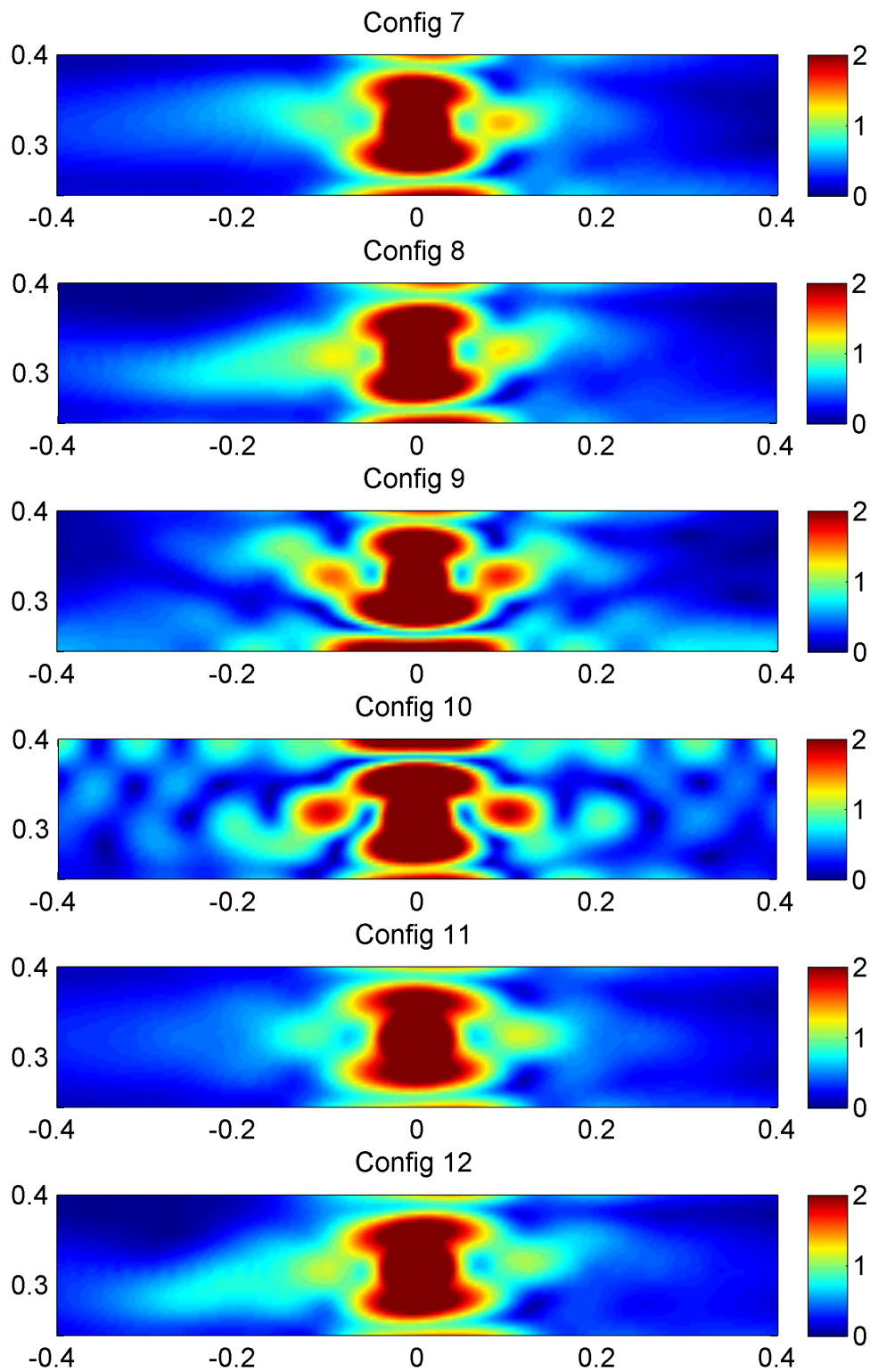


Figure 4. Acoustic pressure amplitude at  $\theta = 0^\circ$ , Configs 7-12.

## VI. Conclusion

A general approach was discussed to calculate Green's functions in a duct with parallel shear flow. It features the numerical integration of the inverse Fourier transform with respect to the axial coordinate. The shear flow is assumed to be piecewise uniform. Bessel functions can be used to evaluate the Green's functions, and issues with continuum modes are circumvented. The range of applicability is wide:

- annular or hollow ducts,
- open jets with or without inner body,
- hard or lined duct walls and inner body walls,
- locally and non-locally reacting liners.

Applications were shown to several configurations.

### Appendix: Source on the axis

When the source is on the axis,  $\rho = 0$ , Eq. (11) does not hold and the shooting method is not applicable. In that case, we can use an alternative shooting method, as described below.

First, it is noted that  $F_m = 0$  for  $m \neq 0$ , because of the axisymmetry. We assume that an “inner radius”  $R_{\text{inner}}$  exists such that the flow properties are uniform for  $r \leq R_{\text{inner}}$ . In that case Eq. (16) holds for  $r > 0$ :

$$\frac{1}{r} \frac{d}{dr} \left( r \frac{dF_0}{dr} \right) + \left( (\omega + U\alpha)^2 / c_0^2 - \alpha^2 \right) F_0 = 0. \quad (44)$$

As in Chapter IV, we shoot from  $r = R_{\text{outer}}$  to  $r = R_{\text{inner}}$ , thus providing an “outer solution”  $v(r)$ . For  $r \leq R_{\text{inner}}$  we write the solution as

$$v(r) = AJ_0(\varepsilon r) + BH_0^{(2)}(\varepsilon r). \quad (45)$$

The parameters  $A$  and  $B$  are found by matching  $v(r)$  and its derivative at  $r = R_{\text{inner}}$ :

$$\begin{cases} AJ_0(\varepsilon R_{\text{inner}}) + BH_0^{(2)}(\varepsilon R_{\text{inner}}) = v(R_{\text{inner}}), \\ AJ_0'(\varepsilon R_{\text{inner}}) + BH_0^{(2)'}(\varepsilon R_{\text{inner}}) = v'(R_{\text{inner}})/\varepsilon. \end{cases} \quad (46)$$

Hence, we have

$$\begin{pmatrix} A \\ B \end{pmatrix} = \frac{\pi i R_{\text{inner}}}{2} \begin{pmatrix} H_0^{(2)'}(\varepsilon R_{\text{inner}}) & -H_0^{(2)}(\varepsilon R_{\text{inner}}) \\ -J_0'(\varepsilon R_{\text{inner}}) & J_0(\varepsilon R_{\text{inner}}) \end{pmatrix} \begin{pmatrix} \varepsilon v(R_{\text{inner}}) \\ v'(R_{\text{inner}}) \end{pmatrix}, \quad (47)$$

where use has been made of a Wronskian for Bessel functions<sup>17</sup>.

Thus, we have obtained a complete “outer solution”  $v(r)$ , which can still be multiplied with a constant  $C$ . This constant is chosen such that

$$BC = \frac{i}{4}. \quad (48)$$

Then we have for  $r \leq R_{\text{inner}}$

$$F_0 = Cv(r) = ACJ_0(\varepsilon r) + \frac{i}{4} H_0^{(2)}(\varepsilon r). \quad (49)$$

The term with the Hankel function is a Green's function in uniform flow; the term with the Bessel function is a solution of the homogeneous equation. From the foregoing, it follows that

$$C = \frac{1}{2\pi R_{\text{inner}} (-\varepsilon J_0'(\varepsilon R_{\text{inner}}) v(R_{\text{inner}}) + J_0(\varepsilon R_{\text{inner}}) v'(R_{\text{inner}}))}. \quad (50)$$

The final solution  $G = G_0$  follows from Eq. (13).

### Acknowledgments

The investigations reported in this paper were carried out within the projects FLOCON and OPENAIR, which are sponsored through the European Community's Seventh Framework Programme (FP7/2007-2013), under grant agreements n° 213411 and n° 234313, respectively.



## References

- <sup>1</sup>Sijtsma, P., "Circular Harmonics Beamforming with Multiple Rings of Microphones," AIAA Paper 2012-2224, June 2012.
- <sup>2</sup>Namba, M., "Three-Dimensional Analysis of Blade Force and Sound Generation for an Annular Cascade in Distorted Flow," *Journal of Sound and Vibration*, Vol. 50, No. 4, 1977, pp. 479-508.
- <sup>3</sup>Schulten, J. B. H. M., "Sound Generated by Rotor Wakes Interacting with a Leaned Vane Stator," *AIAA Journal*, Vol. 20, No. 10, October 1982, pp.1352-1358.
- <sup>4</sup>Ffowcs Williams, J. E., and Hawkins, D. L., "Sound Generation by Turbulence and Surfaces in Arbitrary Motion," *Philosophical Transactions of the Royal Society, A*, Vol. 264, 1969, pp. 321-342.
- <sup>5</sup>Lewy, S., "Prediction of Turbofan Rotor or Stator Broadband Noise Radiation," *Acta Acustica*, Vol. 93, No. 2, 2007, pp. 275-283.
- <sup>6</sup>Casalino, D., and Bodony, D., "Green's Function Discretization of Pridmore-Brown Wave Operator," *Center for Turbulence Research, Proceedings of the Summer Program 2006*, 2006, pp. 547-558.
- <sup>7</sup>Sijtsma, P., "Feasibility of In-Duct Beamforming," AIAA Paper 2007-3696, May 2007.
- <sup>8</sup>Dougherty, R. P., and Walker, B. E., "Virtual Rotating Microphone Imaging of Broadband Fan Noise," AIAA Paper 2009-3121, May 2009.
- <sup>9</sup>Rienstra, S. W., and Tester, B. J., "An Analytic Green's Function for a Lined Circular Duct Containing Uniform Mean Flow," AIAA Paper 2005-3020, May 2005.
- <sup>10</sup>Agarwal, A., Morris, P. J., and Mani, R., "Calculation of Sound Propagation in Non-Uniform Flows: Suppression of Instability Waves," *AIAA Journal*, Vol. 42, No. 1, January 2004, pp. 80-88.
- <sup>11</sup>Dowling, A. P., Ffowcs Williams, J. E., and Goldstein, M. E., "Sound Production in a Moving Stream", *Philosophical Transactions of the Royal Society of London, A*, Vol. 288, 1978, pp. 321-349.
- <sup>12</sup>Rienstra, S. W., "A Classification of Duct Modes Based on Surface Waves," AIAA Paper 2001-2180, May 2001.
- <sup>13</sup>Brambley, E. J., Darau, M., and Rienstra, S. W., "The Critical Layer in Sheared Flow," AIAA Paper 2011-2806, June 2011.
- <sup>14</sup>Goldstein, M. E., *Aeroacoustics*, McGraw-Hill, 1976.
- <sup>15</sup>Pridmore-Brown, D., "Sound Propagation in a Fluid Flowing through an Attenuating Duct," *Journal of Fluid Mechanics*, Vol. 4, 1958, pp. 393-406.
- <sup>16</sup>Myers, M. K., "On the Acoustic Boundary Condition in the Presence of Flow," *Journal of Sound and Vibration*, Vol. 71, No. 3, 1980, pp. 429-434.
- <sup>17</sup>Olver, F. W. J., Lozier, D. W., Boisvert, R. F., and Clark, C. W., *NIST Handbook of Mathematical Functions*, Cambridge, 2010.
- <sup>18</sup>Rienstra, S. W., "Contributions to the Theory of Sound Propagation in Ducts With Bulk-Reacting Lining," *Journal of the Acoustical Society of America*, Vol. 77, No. 5, 1985, pp. 1681-1685.
- <sup>19</sup>Sijtsma, P., and Van der Wal, H. M. M., "Modelling a Spiralling Type of Non-Locally Reacting Liner," AIAA Paper 2003-3308, 2003.
- <sup>20</sup>Miles, J. W., "On the Reflection of Sound at an Interface of Relative Motion," *Journal of the Acoustical Society of America*, Vol. 29, No. 2, 1957, pp. 226-228.
- <sup>21</sup>Ribner, H. S., "Reflection, Transmission and Amplification of Sound by a Moving Medium," *Journal of the Acoustical Society of America*, Vol. 29, No. 4, 1957, pp. 435-441.